Analysis of Torque Data from Friction Stir Welds in Aluminum Alloys

Kevin Colligan
Concurrent Technologies Corporation
Johnstown, PA, USA

Keywords: Joining, Aluminum, Heat generation

Abstract

In the present work, welding procedures for friction stir welding (FSW) of aluminum alloys were collected from published and unpublished reports, permitting analysis of a diverse collection of alloys, material thickness, tool designs and machine parameters. Spindle torque is a key variable in FSW since it is directly related to heat generation. The compiled data set permitted analysis of spindle torque from a wide variety of welding conditions. To compare heat generation from diverse welding procedures, the torque data and welding tool geometries were used to calculate the average contact shear stress during welding, which was analyzed against the average tool surface velocity for each procedure. The results gave insight into the effects of welding speed, rotational speed and alloy on the average flow stress. The results suggested evidence of reaching a minimum flow stress at high tool surface velocities and a possible effect of initial workpiece temper on conditions during welding.

Introduction

FSW has been a topic of research for nearly three decades, and a sizable body of work has been published. Most research has been focused on specific materials, alloys, workpiece thickness, etc., limiting each scope simply as a practical consideration. One exception has been the work by researchers at the University of South Carolina which analyzed welds from a wide spectrum of welding conditions in aluminum alloys 2524, 7050 and others [1-3], all of which included spindle torque measurements. The present work sought to collect data from many published works to examine broad trends, restricting focus only to conventional FSW in aluminum alloys. This data, combined with unpublished procedures, gave insight into heat generation in friction stir welding.

Heat generation is an important parameter in any welding process, as it relates to the effect of welding on the materials being joined, to the productivity of the process and to the energy cost in commercial welding operations, as examples. It is also an indicator of the conditions present during welding. FSW is a fully coupled thermomechanical process, meaning that the material response develops a self-referential balance: heat dissipation preconditions the workpiece material, setting the stage for heat generation in the weld, which then dissipates into the surrounding material. This balance is responsible for the inherent stability of the FSW process. This also means that the heat input is determined by the interaction between the welding tool and the workpiece, and is a response from the process, not a prescribed input to the process. As such, heat generation is an important indicator of what is happening during welding, with the proper analysis.

Researchers have developed various approaches to expressing heat generation in FSW, often as input to models for predicting temperature distribution during welding. The earliest approaches represented the heat as coming from the shoulder only, assuming a circular heat source on the plate surface to calculate heat input from an assumed friction coefficient or based on the workpiece shear flow stress, acting on the shoulder area [4-8]. Analysis of the contact conditions between the tool and matrix followed [12-19], leading to the conclusion that heat generation could be best represented as being based on the shear flow stress acting on all tool surfaces. In 2002, an important analytical step was made by relating the spindle torque to the shear flow stress of the matrix, assuming a uniform average flow stress distributed over the tool surfaces [12, 13].

A detailed analysis was developed by Schmidt, et al., [14] to rationalize the tool/matrix contact shear stress value based on different categories of contact conditions, including sticking, sliding, and mixed sticking/sliding. In the case of sliding, the defined condition is one of relative motion between the tool and the workpiece with the workpiece not sufficiently stressed to cause deformation. The case of sticking was defined such that there was

seizure between the tool and the workpiece, resulting in matrix deformation at the local velocity of the tool at the contact interface, with decaying velocity moving away from the interface. Finally, the case of mixed sticking/sliding was defined such that the matrix material is deforming at the contact interface at a speed that was less than the local tool velocity and was thus sliding relative to the tool but was deforming, nonetheless. In these latter two cases, the contact stress was rationalized to be equal to the shear flow stress of the matrix – the difference between the two cases being the velocity of the matrix at the contact interface.

According to Schmidt, the contact conditions in FSW of aluminum generate plastic deformation over most of the tool surfaces, except for a small region at the periphery of the shoulder, where frictional heating generates very close to the same heat as the sticking condition. These conclusions confirm the assumption made in the input torque model approach, that the spindle torque results from contact shear flow stress that is uniformly distributed over the tool. This is the approach taken for analysis of spindle torque and welding tool geometry data from the data set.

Data Set

Data was collected from published and unpublished sources [16]. All welding procedures represented conditions that produced void free welds, which may or may not have been optimized to any criteria. All procedures were for aluminum alloys welded using conventional, single-sided FSW. A total of 170 procedures, representing 20 different alloys in various tempers, were included, 134 of which included spindle torque data. The complete data set is available for download, with references included [17].

Analytic Approach

Spindle Torque Analysis

The shear yield stress is calculated by dividing the measured spindle torque by the surface integral of the radius,

$$\tau_{yield} = \frac{T}{\int_S r\, dA} = \frac{T}{geo} \tag{1}$$

where T is the spindle torque and S is the total surface of the tool, including the shoulder, the probe sides and the probe end. The surface integral is referred to as "*geo*" since it comprises the geometry of the welding tool. To derive *geo*, an assumption was made of a concave or flat shoulder, a frustrum or cylindrical probe and a flat probe tip. The incremental areas for each region of the tool surface are,

$$\begin{aligned} shoulder\ incremental\ area &= \frac{r}{\cos\alpha} dr d\theta \\ probe\ side\ incremental\ area &= \frac{r}{\cos\beta} dz d\theta \\ probe\ tip\ incremental\ area &= r\, dr d\theta \end{aligned} \tag{2}$$

where,

$\alpha = shoulder\ concavity\ angle$
$\beta = frustum\ probe\ half\ angle$
$S = shoulder\ radius$
$P_R = probe\ root\ radius$
$P_T = probe\ tip\ radius$
$r = dimension\ in\ radial\ direction$
$z = dimension\ along\ probe\ axis$
$t = workpiece\ thickness, or\ probe\ length$
$\theta = anglular\ position$

The radius dimension to the probe side is related to the coordinate along the probe axis, z, using the expression $r = (P_R - z\tan\beta)$. Then, noting that $dA = r\,dr d\theta$,

$$geo = \int_S r\,dA = \int_0^{2\pi}\int_{P_R}^{S}\frac{r^2}{\cos\alpha}dr\,d\theta + \frac{1}{\cos\beta}\int_0^{2\pi}\int_0^{t}(P_R - z\tan\beta)^2\,dz\,d\theta + \int_0^{2\pi}\int_0^{P_T} r^2 dr\,d\theta \quad (3)$$

For cylindrical probes, P_T is set equal to P_R, and β is set to zero, for flat shoulders, α is set to zero. Performing the integrations yields,

$$geo = \frac{2\pi}{3}\left[\frac{S^3 - {P_r}^3}{\cos\alpha} + \frac{t((P_R + P_T)^2 - P_R P_T)}{\cos\beta} + {P_T}^3\right] \quad (4)$$

Combining equations (1) and (4),

$$\tau_{yield} = \frac{T}{\frac{2\pi}{3}\left[\frac{S^3 - {P_r}^3}{\cos\alpha} + \frac{t((P_R + P_T)^2 - P_R P_T)}{\cos\beta} + {P_T}^3\right]} \quad (5)$$

Finally, the normal flow stress is calculated from the shear flow stress using the von Mises yield criterion,

$$\sigma_{yield} = \tau_{yield}\sqrt{3} \quad (6)$$

Equations (5) and (6) were used to calculate the flow stress for each welding procedure in the data set that included torque data, enabling study of flow stress variation as a function of average surface velocity for many different conditions, as will be presented in the following section.

Surface Velocity Analysis

Representation of the surface velocity has taken various forms in the literature, including surface velocities developed from the radius of the probe or the shoulder. Long, et al. [18] examined spindle torque as a function of tool rotation speed, which sufficed for evaluation of torque from a single welding tool design. Since the present study regarded torque measurements from a wide variety of welding tool geometries, it was necessary to develop a basis for comparison that comprised the essential tool features.

In the present study, an area-based average surface velocity was expressed as the velocity of an increment of area, integrated over the area, and divided by the total area. Imagine a function of surface velocity plotted against surface area, shown in Figure 1.

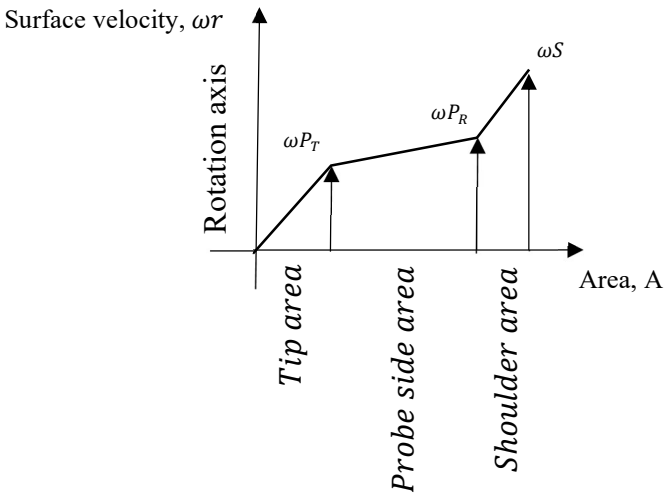

Figure 1. Surface velocity as a function of area.

The average of this function is given by,

$$\text{Average surface velocity} = \omega\bar{r} = \frac{\omega \int_S r\, dA}{total\ surface\ area} \tag{7}$$

The double integral in the numerator is equal to *geo*, from equation (4), so,

$$\omega\bar{r} = \omega \frac{geo}{total\ area} \tag{8}$$

resulting in,

$$\omega\bar{r} = \omega \left[\frac{\frac{2}{3}\left[\frac{S^3 - {P_R}^3}{\cos\alpha} + \frac{t((P_R + P_T)^2 - P_R P_T)}{\cos\beta} + {P_T}^3\right]}{\frac{(S + P_R)(S - P_R)}{\cos\alpha} + \frac{t(P_R + P_T)}{\cos\beta} + {P_T}^2} \right] \tag{9}$$

Results and Discussion

The flow stress, according to equations (5) and (6), was plotted as a function of average surface velocity from equation (9), as shown in Figure 2. The data suggests a bi-linear relationship. This relationship was reported by Long, et al. [16], based on welds made with variable spindle speed in aluminum 2219, 5083 and 7050. In that case, welds were made in three alloys with continuously increasing spindle speed. Flow stress was calculated using the input torque method, as was done in the present study, then plotted as a function of spindle speed. Spindle speed is equivalent to surface velocity for a group of welds made with an identical welding tool geometry. Similarly, a bi-linear relationship between peak temperature and spindle speed was reported by Sato, et al. [19], in alloy 6063 aluminum. In both cases, a grain size plateau was reported at about the same rotational speed as a distinct flattening of the torque curve and the maximum temperature curve, respectively. Further increase in rotation speed gave diminished increase in grain size and peak temperature, with diminished decrease in torque. In these studies, the plateau in grain size was concluded to be an artifact of having reached a plateau of peak temperature since the grain growth was consistent with static recrystallization from a peak temperature. These results suggest a depletion of heat generation capacity as rotational speed is increased. The results presented in Figure 2 suggest that this phenomenon may be present in many aluminum alloys during FSW. Note that two welding procedures in 7075 aluminum were excluded from the least squares calculation for reasons given below.

Details from specific alloys provide further insight. Average flow stress data for Al alloy 5456-H116, 5083-H131 and 5083-O plates are presented as a function of average surface velocity in Figure 3, using spindle torque data from unpublished results by the author from Concurrent Technologies Corporation (aluminum 5456 and 5083), published results by the author [21] and published results from the University of South Carolina [2]. The aluminum 5456 welds were made as part of a study that produced welds with pre-rotation defects [20]. Resolution of the defects involved reducing the shoulder diameter, from about 35.6 mm to 30.5 mm. Five travel speeds and two rotational speeds were used for each tool. As can be seen in the figure, travel speed had the effect of increasing the flow stress, while increasing the spindle speed had the effect of decreasing the flow stress. These effects have been noted elsewhere [16, 2, 21]. A similar trend was discernable in the 7050 data, presented below. It is also notable that the welds in 5083-O made at low surface velocity had lower flow stress than the other 5XXX alloy welds, suggesting a lingering effect of the initial material condition, which was less pronounced at higher surface velocity and travel speed. Procedures in 7050 and 7075 O temper did not exhibit this temper effect. The range of average surface velocity in the test data was insufficient to demonstrate a certain agreement with heat-treatable alloys at high surface velocity.

Flow stress data from welds made in 2524-T351 are presented in Figure 4. Here, there was close agreement with a bi-linear characterization. It is interesting that the slopes of the bi-linear characterization and the intersection of the trends differ significantly from the all-alloy average behavior, although no explanation for this result is given.

Flow stress data for Al alloy 7050 are presented in Figure 5. The current data set for Al alloy 7050 was extracted from work at the University of South Carolina, except for a single welding procedure in 39.4 thickness material, indicated in the figure [from unpublished results by the author at Concurrent Technologies Corporation]. In the current analysis, alloy 7050 welding procedures indicated a crossing point in the linear trends at a surface velocity of 0.305 m/s, compared to Long's result, 0.224 m/s, from three alloys.

Two outliers in the 7050 data are notable. One outlier was from a weld in 32 mm thickness that exhibited low flow stress. Apparently, the high thickness alone was not responsible for the low flow stress, since the weld in 39.4 mm material agreed with welds in thinner material. It is notable that the weld in 32 mm material was made at a lower travel speed, 0.9 mm/s, compared to 1.3 mm/s in the 39.4 mm material. The lower flow stress would be consistent with lower travel speed, as discussed above, but the size of the effect is greater than observed in thinner materials. A second outlier came from a pair of welds made in 7075-T6 material at very high travel speed, 8.5 mm/s. The size of the effect of travel speed was much higher than that observed in 5456 aluminum, likely because the travel speed was so much higher. These high travel speed welds may represent conditions where material flow is contributed to by forcible extrusion around the probe. Further research into flow stress variation with travel speed is needed.

It was tempting to surmise from the general trend of the data in Figure 2 that there may have been a continuous inverse relationship between flow stress and surface velocity. However, examination of the details from Al alloys such as 2524 and 7050, combined with published results from Long and Sato mentioned above, suggest that some step-change occurs, producing a discontinuous relationship. This step change may simply due to approaching the melting point of the matrix. Further research is needed to explore this in detail for different aluminum alloys.

Conclusions

Welding procedures from published and unpublished sources were collected and analyzed to extract useful trends in the data. Analysis of torque from the data set gave insight into the response of various aluminum alloys to the conditions of welding. When plotted against average tool surface velocity, a bi-linear relationship was observed. Average flow stress values of 20 MPa to 60 MPa were most common. The results confirm observations from other researchers, with a more extensive data set than existed previously, and suggest further research into the depletion of heat generation at elevated surface velocities and the effect of travel speed on flow stress during welding.

The results suggest control strategies for closed-loop welding control systems. For example, it may be reasonable for a controller to limit the rotational speed to a level where an average surface velocity of 0.3 m/s is reached, since further increase in rotational speed yields limited additional heat generation for the travel speeds studied. Further, the welding controller may command a welding speed increase or rotational speed decrease if the spindle torque drops to a point where the minimum flow stress for a specific alloy is reached, generally around 20 MPa. Such a drop in torque may result from a change in thermal boundary conditions, such as from welding past some change in workpiece geometry, for example.

References

1. Yan, Junhui, Suttton, M.A. and Reynolds, A.P., "Process-structure-property relationships for nugget and heat affected zone regions of AA2524-T351 friction stir welds," Science and Technology of Welding & Joining, December 2005.
2. Reynolds, A.P. and Tang, W., "Alloy, Tool Geometry, and Process Parameter Effects on Friction Stir Weld Energies and Resultant FSW Joint Properties," Friction Stir Welding and Processing, K.V. Jata, M.W. Mahoney, R.S. Mishra, S.L. Semiatin, and D.P. Field, eds., TMS, Warrendale, PA, 2001, pp. 15–23.

3. Reynolds, A., Tang, W., Khandkar, Z., Khan, J.A., and Lindner, K., "Relationships between Weld Parameters, Hardness Distribution and Temperature History in Alloy 7050 Friction Stir Welds," Science and Technology of Welding and Joining, 2005, Vol. 10, No. 2, pp. 190–199.
4. Russell, M.J. and Shercliff, H.R., "Analytical modelling of friction stir welding," Proc. INALCO '98: 7th Int'l. Conf.: Joints in Aluminum, Vol 2, pp.185-217, Cambridge, UK, 16 April, 1998.
5. Frigaard, O., Grong, O. and Midling, O.T., "Modelling of heat flow phenomena in friction stir welding of aluminum alloys," Proc. INALCO '98: 7th Int'l. Conf.: Joints in Aluminum, Vol 2, pp.185-217, Cambridge, UK, 16 April, 1998.
6. McClure, J.C., Tang, W., Murr, L.E., Guo, X., Feng, Z. and Gould, J.E., "Thermal model in friction stir welding," 5th Int'l. Trends in Welding Research Conference Proceedings, 1-5 June, 1998, Pine Mountain, GA, ASM Int'l, pp. 590-596, 1998.
7. Russell, M.J. and Shercliff, H.R., "Analytical modelling of microstructure development in friction stir welding," 1st International Symposium on Friction Stir Welding, Thousand Oaks, CA, 14-16 June, 1999.
8. Chao, Y.J. and Qi, X., "Heat transfer and thermo-mechanical analysis of friction stir joining of AA6061-T6 plates," 1st International Symposium on Friction Stir Welding, Thousand Oaks, CA, 14-16 June, 1999.
9. Colegrove, P., "3 dimensional flow and thermal modelling of the friction stir welding process," 2nd International Symposium on Frictioin Stir Welding, Gothenburg, Sweden, 28-28 June 2000.
10. Xu, S., Deng, X., Reynolds, A.P. and Seidel, T.U., "Finite element simulation of material flow in friction stir welding," Sci. Tech. Weld. and Join., 2001, Vol. 6, No. 3, pp. 191-193.
11. Song, M., Kovacevic, R., Ouyang, J., and Valant, M., "A detailed three-dimensional transient heat transfer model for friction stir welding," 6th Int'l. Trends in Welding Research Conference Proceedings, 15-19 April, 2002, Pine Mountain, GA, ASM Int'l., pp. 247-252, 2003.
12. Khandkar, M.Z.H., Khan, J.A. and Reynolds, A.P., "Input torque based thermal model of friction stir welding," 6th Int'l. Trends in Welding Research Conference Proceedings, 15-19 April, 2002, Pine Mountain, GA, ASM Int'l., pp. 218-223, 2003.
13. Khandkar, M.Z.H., Khan, J.A. and Reynolds, A.P., "Prediction of temperature distribution and thermal history during friction stir welding: input torque based model," Science and Technology of Welding and Joining, 2003, Vol. 8, No. 3, pp. 165-174.
14. Schmidt, H., Hattel, J. and Wert, J., "An analytic model for the heat generation in friction stir welding," Modelling and Simulation in Materials Science and Engineering, 2004, Vol. 12, pp. 143-157.
15. Schmidt, H. and Hattel, J., "A local model for the thermomechanical conditions in friction stir welding," Modelling Simul. Mater. Sci. Eng., 13 (2005) 77-93.
16. Colligan, K., (2022) Analysis of data from friction stir welds in aluminum. Paper presented at the 2022 International Symposium on Friction Stir Welding and Processing, Luneburg, Germany, 28-30 September, 2022
17. https://www.ctc.com/public/solutions/techandinnovation/friction-stir-welding.aspx
18. Long, T., Tang, W. and Reynolds, A.P., "Process response parameter relationships in aluminum alloy friction stir welds," Sci. & Tech. of Weld. And Join., 2007, vol. 12, no. 4, 311-317.
19. Sato, Y.S., Urata, M. and Kokawa, H., "Parameters controlling microstructure and hardness during friction stir welding of precipitation-hardenable aluminum alloy 6063," Metallurgical and Materials Transactions A, Vol. 33A, pp. 625-635, March 2002.
20. Colligan, K., "Description of a pre-rotation defect in friction stir welding of 5456 aluminum," 8th International Symposium on Friction Stir Welding, Timmendorfer Strand, Germany, May 18–20, 2010.
21. Colligan, K.J., Xu, J., Pickens, J.R., "Welding Tool and Process Parameter Effects in Friction Stir Welding of Aluminum Alloys," Friction Stir Welding and Processing II, K.V. Jata, M.W. Mahoney, R.S. Mishra, and T. Lienert, eds., TMS, Warrendale, PA, 2003, pp. 181–190.

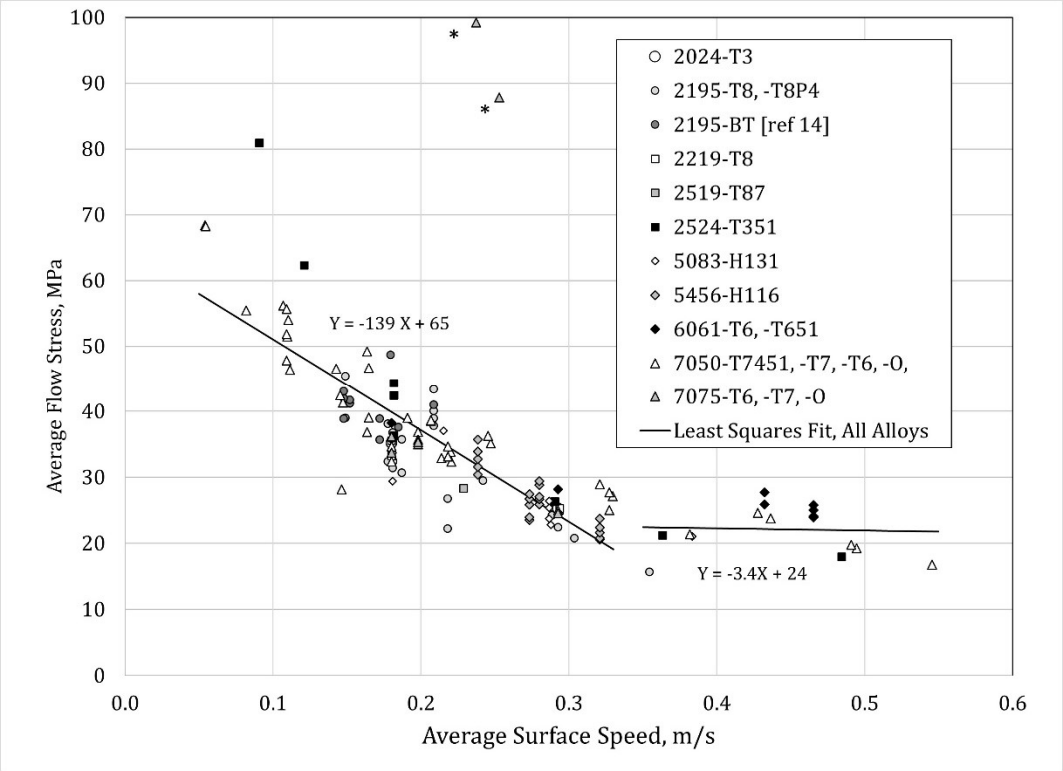

Figure 2. Flow stress as a function of average surface speed, all alloys.
**Indicates two procedures excluded from least squares fit.*

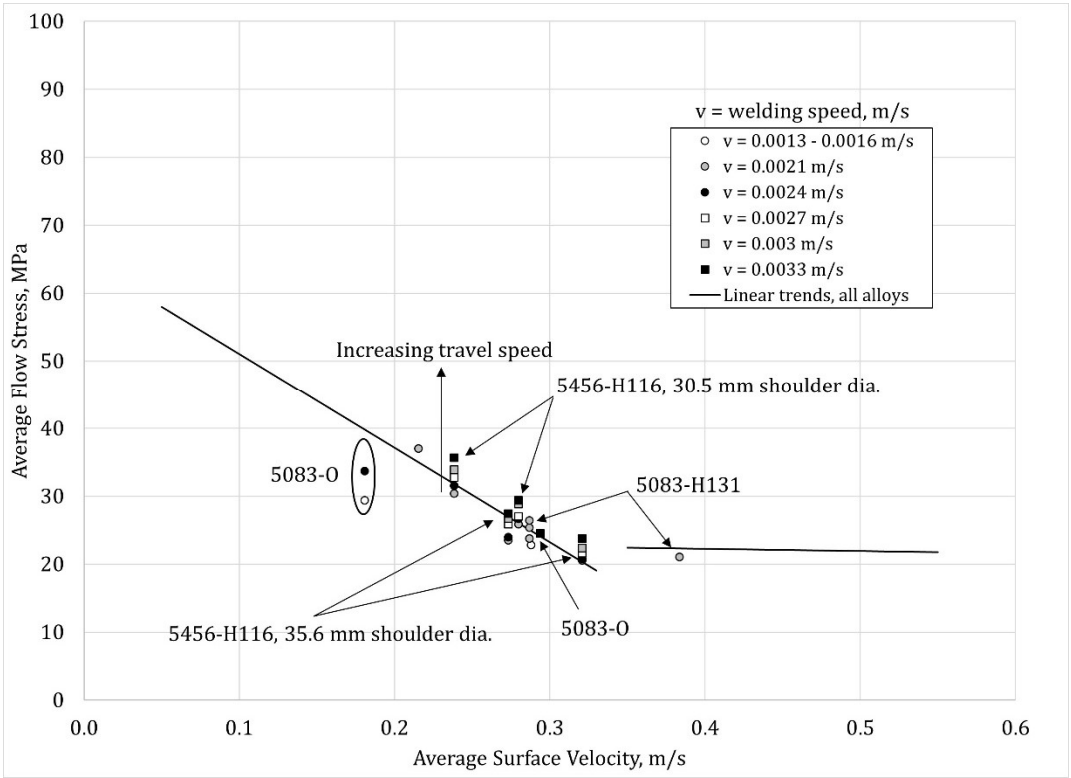

Figure 3. Flow stress for 5456-H116 and 5083-O, -H131.

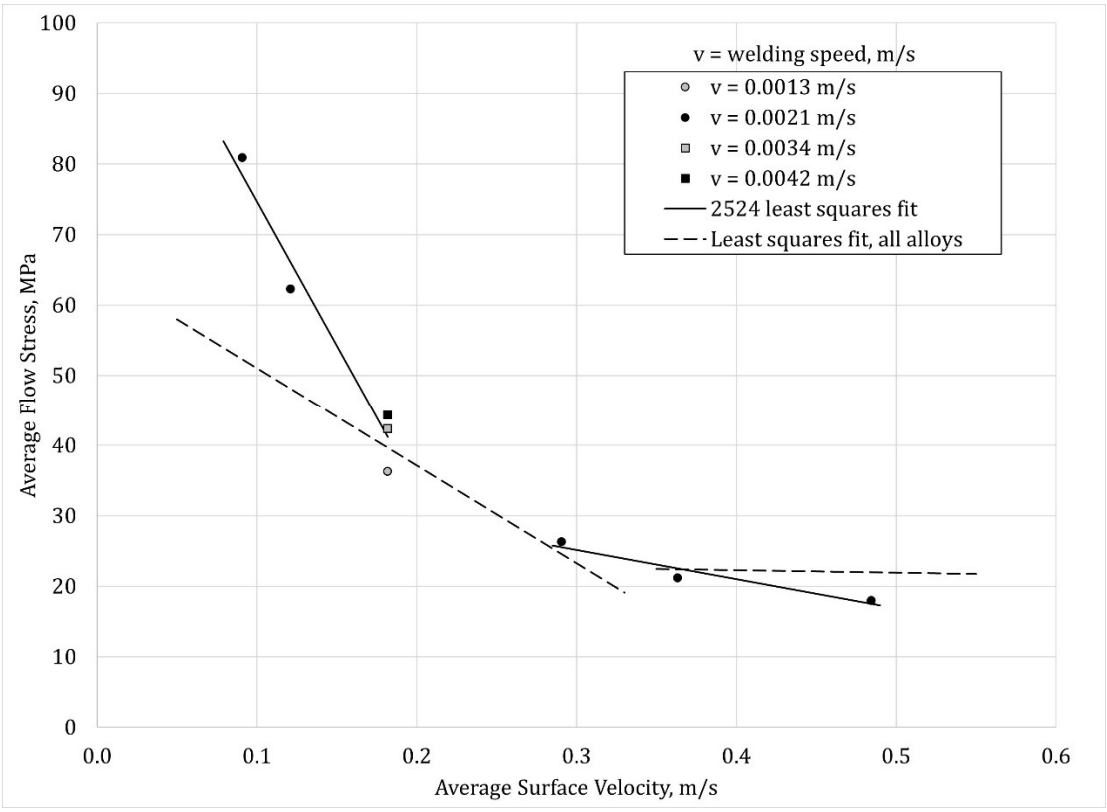

Figure 4. Flow stress for 2524-T351.

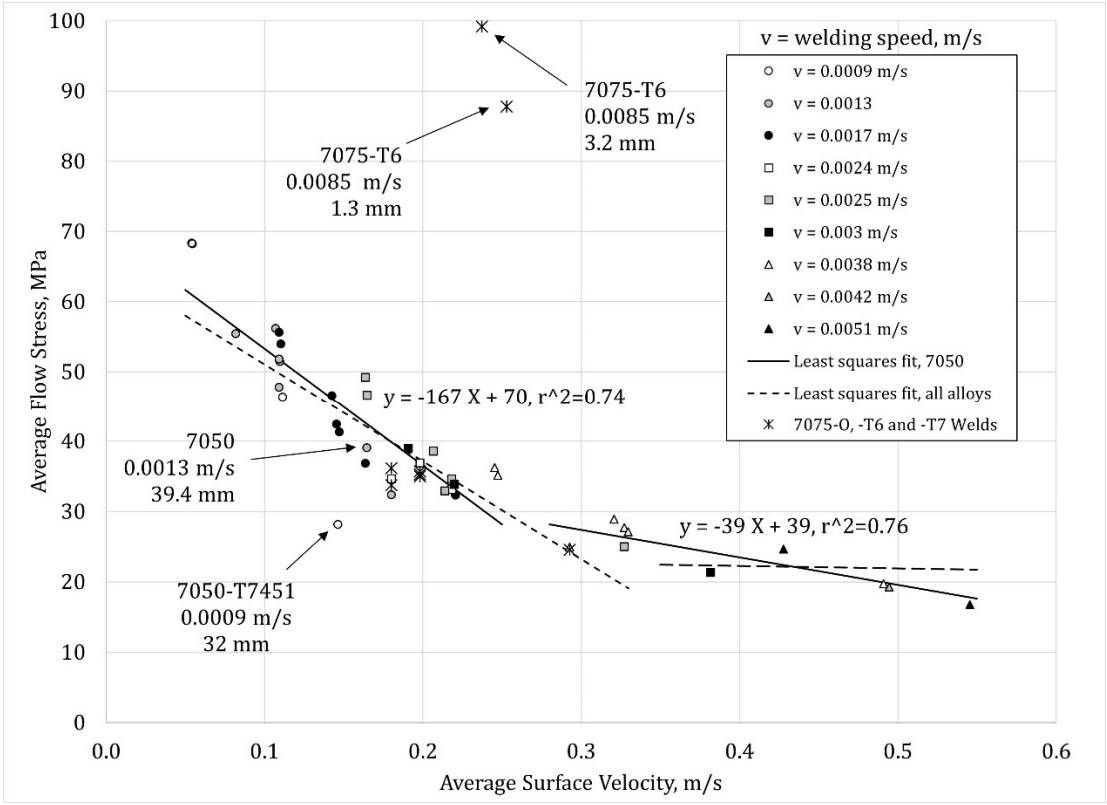

Figure 5. Flow stress for 7050-O, -T7and -T7451 with 7075-O, -T6 and -T7, for comparison.